Infrared Visualization for Sensor Calibration

Rocky Ratia

***Abstract* — Autonomous robots, such as those competing in the Botball competition, rely on infrared (IR) distance and reflectance sensors for navigation and alignment. However, because the IR wavelengths are invisible to the human eye, it can be challenging to align and calibrate these sensors. This paper introduces a cost-effective framework, utilizing a modified camera. By removing the camera's built-in wavelength filter, the proposed system visually reveals the apparent orientation, beam pattern, and coverage of the infrared emitters. Testing demonstrates that this method improves the accuracy and repeatability of IR sensor alignment, simplifying calibration for tasks such as line following and obstacle detection.**

I. Introduction

Teams are provided with a multitude of sensors for use in the official Botball kit. The kit provides teams with a distance sensor and two sizes of surface reflectance sensors. All of these sensors make use of infrared light, or IR, to calculate their values. As a result, calibrating and orienting these sensors for optimal usage can be tricky due to the invisible nature of IR light. Because the IR spectrum is invisible to the human eye, verifying the sensing region or spatial footprint of these sensors during assembly and testing can be challenging. The physical design of these sensors makes mounting them a substantial struggle, especially during the rapid prototyping phase. To address this difficulty, this paper introduces a low-cost visual alignment framework utilizing a high-resolution full-spectrum reference camera for positional and orientation verification of an IR sensor.

II. Distance Sensor Characteristics

While no official part number is directly provided by KIPR, older provided distance sensors had "SHARP 2Y0A21 F 8Y" printed on the casing, showing that the IR distance sensor is based on the GP2Y0A21YK0F analog distance sensor. This sensor utilizes an IR LED, a Position Sensitive Detector (PSD), and a built-in signal processor circuit to read distances with reduced sensitivity to the object's color or reflectivity [1]. While the internal processing handles color and reflectance variations reasonably well, the sensor exhibits several characteristics that present challenges for autonomous robots. Namely, as shown in Fig. 1, the distance to the object being viewed is non-linear.

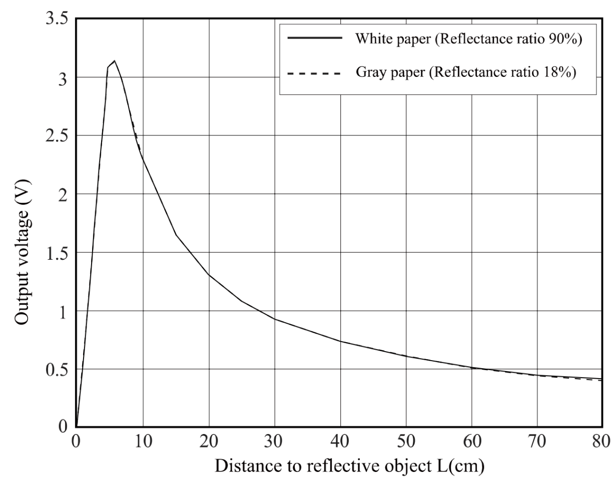

Fig. 1. The official datasheet graph of distance to object versus output voltage.

The triangulation method substantially reduces the influence of target color and reflectivity, though the mapping between output voltage and distance itself follows a structure similar to inverse functions, decreasing nonlinearly with distance [1]. This can make differentiating between far objects challenging due to the change between values being smaller. In addition, within the first 15cm of sensor readings, the values sharply spike, which can make differentiating between very close and very far objects challenging. Although the sensor may initially appear to operate similarly to a laser rangefinder, the infrared emitter is an LED rather than a laser diode [1]. The nature of this LED's projection is approximately a square with a circle cut out (as seen in Fig. 2), and because it is a projection, this illuminated region expands the farther from the sensor it is, as shown in Fig. 2. This can cause objects near the edge of the intended location to contribute reflections to the received signal, complicating interpretation of the measurement.

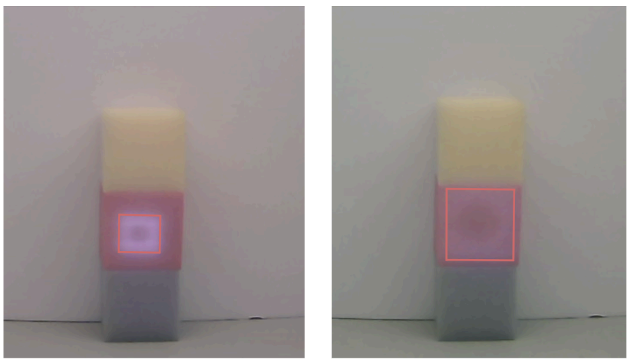

Fig. 2. Side-by-side comparison of the IR LED projection size at a distance of 20 inches (left) and 40 inches (right) from the cube surface. The outlined IR projection becomes visibly larger with increased distance due to the divergence of the LED beam.

III. Reflectance Sensor Characteristics

Alongside the distance sensor, teams may optionally use an IR reflectance sensor. There are three models of line sensors available. Similar to the distance sensor, KIPR themselves did not provide direct part numbers, but “QRD1114 K52”, “EE SB5”, and “EE SF5” are printed on the casings of each model respectively. The smaller line sensor model, the “QRD1114”, consists of an infrared LED and a silicon phototransistor mounted side by side [2]. It also features a daylight filter, which serves to prevent false readings due to sunlight intervention [2]. There are two competition legal large sensor models. The older model, from kits dating to pre-2025, is the model “EE SB5”. It ships as a 4 pin component, working in a similar manner to the “QRD1114”, via an IR LED and silicon phototransistor [3]. The most notable difference between this model and the smaller model is the width of the sensor itself, being able to sense a larger range of values horizontally. The newer sensor model, labeled “EE SF5”, features many of the same features as its predecessor, with the same structure [4]. The most notable difference is in the physical sensor construction, the newer model lacking the “wings” that poke out of either side. While not explicitly stated in the datasheet, experimental observations indicate that both models may have some sort of sunlight filter or compensation logic, neither of which seem to be affected by sunlight through the ambient environment.

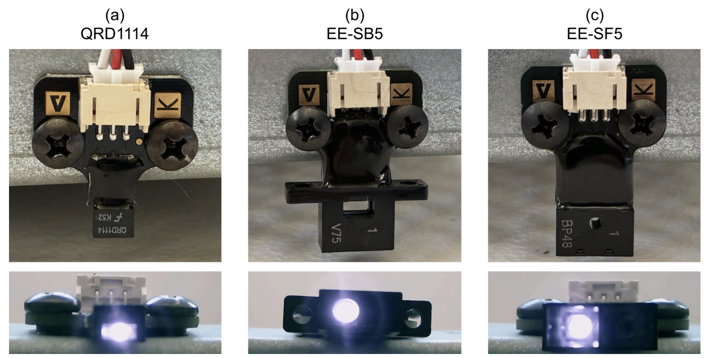

Fig. 3. Reflective infrared sensors evaluated in this work: (a) QRD1114, (b) EE-SB5, and (c) EE-SF5. The upper row shows the sensors mounted on a standard robot chassis. The lower row shows the infrared emitters operating as viewed by a full-spectrum camera.

IV. Full-Spectrum Camera Modification and Setup

Standard consumer cameras utilize a silicon-based image sensor that is sensitive to both visible and infrared light. However, the sensor only receives light that passes through an IR blocking filter, which prevents most infrared wavelengths from reaching the sensor. By removing this filter, the camera becomes capable of visually capturing the wavelengths emitted by the sensors.

Through this modification, the camera is able to display both the robot in its entirety alongside the sensors, in addition to the surface that they are actively scanning. The setup for testing consists of the modified camera positioned on a fixed mount, viewing the robot and its sensors.

The camera used was an Adesso CyberTrack H4 camera. The screws at the back of the camera grant access to the internal cavity, providing access to the filter, as shown below in Fig. 4.

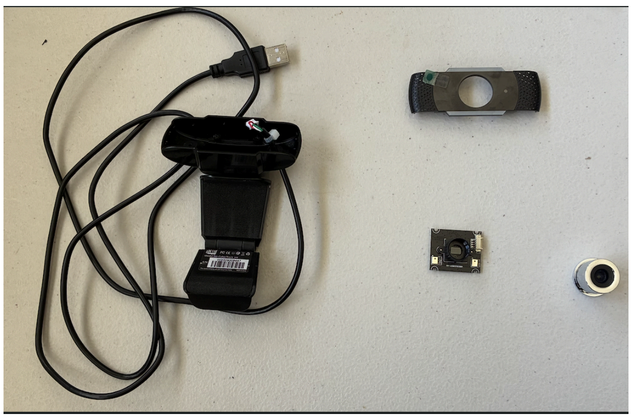

Fig. 4. Teardown view showing the internal structural and electronic components of the camera.

After removing the filter and reassembling the camera, it remains fully functional. It functions just as it did before the modification, retaining plug-and-play functionality. Though the colors are less vibrant, the camera video quality stays constant. The loss of vibrancy occurs because infrared wavelengths contribute to the sensor response across multiple color channels, causing IR light to appear grayscale. Re-inserting the filter causes the camera to return to normal vision. This process can be repeated on any webcam that has the filter separate from the sensor, though testing was done only on the CyberTrack H4 specifically.

V. Alignment Accuracy Test

To evaluate the accuracy of the proposed alignment framework, controlled alignment trials were conducted using a fixed target. A 3 in × 3 in target was mounted at a fixed location on a flat wall. The SHARP distance sensor was mounted on a rotatable chassis with a multi-axis pivot mount, allowing unrestricted adjustment of its orientation. A full-spectrum camera was positioned directly behind the sensor and aligned toward the target. Participants were instructed to align the IR distance sensor with the center of the target under three experimental conditions: without any visual aid, using a fixed reference grid mounted beneath the sensor, and using the live view from the full-spectrum camera. Three participants each completed two alignment attempts under all three conditions, resulting in 18 total alignment trials. The results are presented in Fig. 5, with camera-assisted alignment achieving the lowest mean error and standard deviation compared to all other evaluated alignment methods.

Camera-assisted alignment produced the lowest alignment error across all evaluated methods. Without visual assistance, participants exhibited the largest deviation from the target center. The chassis-grid method reduced the average error by providing a fixed, physical reference for sensor alignment; however, it remained limited by the inability to directly observe the IR projection. The camera-assisted method reduced both the mean error and the standard deviation between alignments, demonstrating improved trial-to-trial repeatability. These results indicate that directly visualizing the IR emission pattern provides a more reliable alignment reference than indirect physical approximations.

VI. Practical Application

The framework reduces ambiguity during debugging by allowing developers to directly observe the illuminated region of each sensor. During line-following calibration, this enables verification that the sensing region overlaps the intended portion of the line. For distance sensing, the visualization assists in confirming that the intended obstacle lies within the illuminated region.

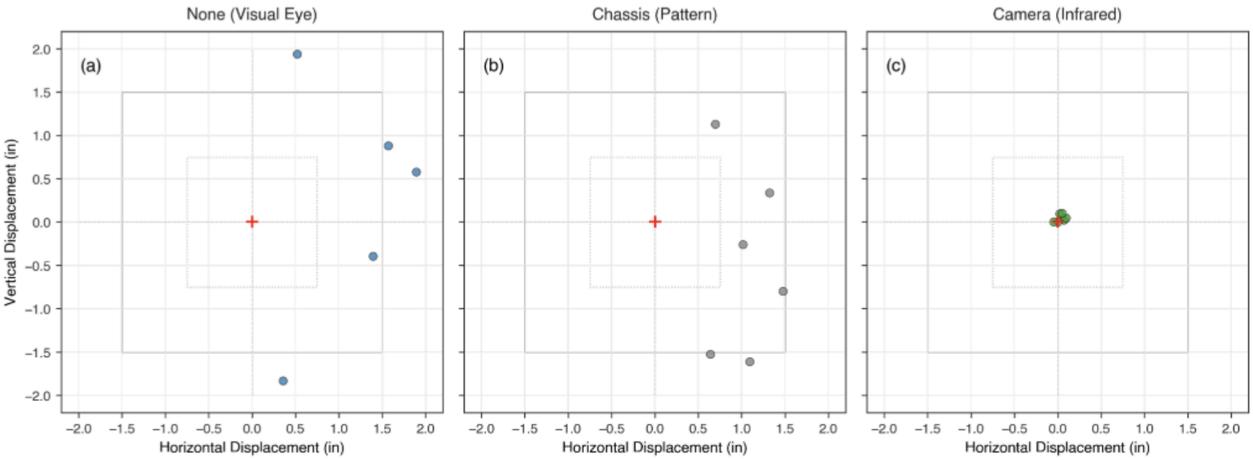

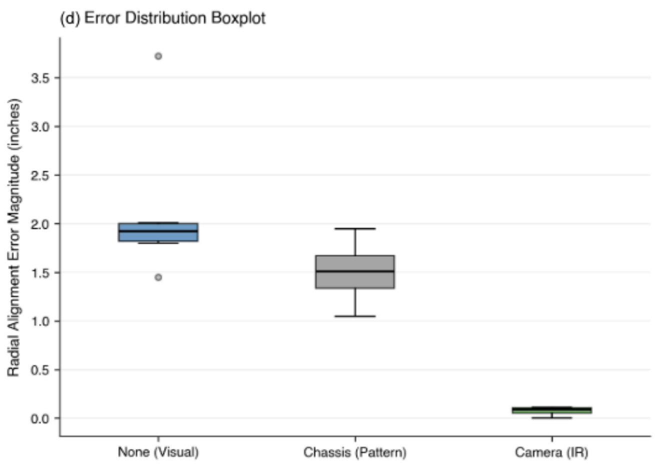

(b) Consolidated Sensor Metrics Summary

Method	Mean (in)	Std Dev (σ)	Max (in)
None (Visual)	2.138	0.731	3.721
Chassis (Pattern)	1.502	0.291	1.946
Camera (IR)	0.073	0.040	0.110

(f) Relative improvement of camera-assisted alignment

Comparison	Mean Error Reduction	Std. Dev. Reduction	Max Error Reduction
Camera vs No Visual Aid	96.6%	94.6%	97.0%
Camera vs Chassis-Grid	95.1%	86.4%	94.3%

Fig. 5. Results of the alignment trials. (a–c) Measured alignment coordinates relative to the center of the target for the no-aid, chassis-grid, and camera-assisted trials, respectively. (d–e) Summary of the alignment error metrics. Camera-assisted alignment achieved the lowest mean error, standard deviation, and maximum error, followed by the chassis-grid alignment, while the unaided trial produced the largest errors. (f) Relative reduction in alignment error metrics achieved by camera-assisted alignment compared with alternative alignment methods.

VII. Limitations

The proposed framework visualizes emitted infrared light but does not directly measure sensor response characteristics or guarantee optimal calibration. Various manufactured batches of sensors respond differently to values, and changes in the supplied voltage by the Wombat can cause sensor values to fluctuate or bias in a direction. Furthermore, evaluation was performed using a single camera model, and compatibility with other cameras depends on the construction of their infrared blocking filters, as well as the sensitivity of the silicon sensor within. In addition, the alignment study was conducted with three participants and therefore serves as an initial validation of the proposed framework rather than a comprehensive human-factors evaluation.

VIII. Conclusion

Proper sensor orientation is essential for an autonomous robot to function correctly. The sensors provided by KIPR offer limited visibility into their sensing regions. An inexpensive consumer webcam can be modified to visualize the emitted infrared light, providing a practical tool for sensor alignment and debugging. This paper presents a cost-effective method for visualizing infrared emissions and improving the alignment of IR sensors.

References

[1] Sharp Corporation, "GP2Y0A21YK0F Distance Measuring Sensor Unit," Datasheet [Online]. Available: https://global.sharp/products/device/lineup/data/pdf/datasheet/gp2y0a21yk_e.pdf

[2] onsemi, "QRD1113, QRD1114: Reflective Object Sensor," Datasheet, Rev. 6, [Online]. Available: https://www.onsemi.com/download/data-sheet/pdf/qrd1114-d.pdf

[3] Omron Corporation, "EE-SB5/SB5-B Photomicrosensor (Reflective)," Datasheet, [Online]. Available: https://omronfs.omron.com/en_US/ecb/products/pdf/en-ee_sb5.pdf

[4] Omron Corporation, "EE-SF5 Photomicrosensor (Reflective)," Datasheet, [Online]. Available: https://omronfs.omron.com/en_US/ecb/products/pdf/en-ee_sf5.pdf